Acoustic data from the spring 2011 bowhead whale census at Point Barrow, Alaska

C.W. Clark[1], R.A. Charif[1], D. Hawthorne[1], A. Rahaman[1], G.H. Givens[2], J.C. George[3] and C.A. Muirhead[1]

Contact e-mail: geof@geofgivens.com

ABSTRACT

Arrays of bottom-mounted passive acoustic recorders were used to continuously record the sounds of bowhead whales migrating past Point Barrow, Alaska for a period of 105 days in April–July 2011, spanning the duration of the visual census. Recorders were deployed in a roughly linear array configuration near the edge of the shorefast ice bordering the open lead. The recorded acoustic data were analysed from 156 sample periods comprising a total of 331 hours coincident with the visual census. Bowhead sounds in the sample periods were found by manual inspection of multi-channel sound spectrograms of the array recordings. Source locations for bowhead sounds that were received on three or more sensors within the array were calculated using a robust localisation algorithm. Very high levels of bowhead acoustic activity were observed in comparison to recording efforts undertaken during past censuses, including high rates of singing and call sequences. A total of 22,426 bowhead sounds yielded 15,647 reliable locations. Of these, 6,944 were within the rectangular aperture zone directly in front of the array and therefore used in the calculation of a new population estimate. This paper summarises one of three critical component of the research program leading to the 2011 estimate of abundance of Givens *et al.* (2016) and is therefore a cornerstone of the scientific basis for IWC Scientific Committee advice for this whale stock.

KEYWORDS: ARCTIC; WHALING-ABORIGINAL; SURVEY-ACOUSTIC; ACOUSTICS; MIGRATION

INTRODUCTION

During the spring, bowhead whales, *Balaena mysticetus*, from the Bering-Chukchi-Beaufort (BCB) population migrate past Point Barrow, Alaska, USA, en route from wintering areas in the Bering Sea to summer feeding grounds in the Beaufort Sea.

Since 1984, the census of the BCB population during its spring migration past Point Barrow has included an acoustic monitoring component combined with a visual survey effort (Clark *et al.,* 1986; Clark *et al.,* 1996; George *et al.,* 2004). In 2011, between 12 April and 7 June, the North Slope Borough's Department of Wildlife Management successfully completed a combined acoustic-visual census. The acoustic monitoring effort, conducted from mid-April through late July, used arrays of passive acoustic recording devices to continuously record underwater sounds. The primary objective of the acoustic study was to detect and locate vocalising bowheads throughout their migration past Point Barrow, Alaska in order to estimate the proportion of acoustically located whales that swam within 4km of the perch from which the visual census was conducted. An important benefit of this study is that it continues the acoustic component of a long-term research project in which both visual observation and acoustic monitoring were collected. As a result, some basic comparisons of acoustic results are available over a span of 27 years.

This paper describes the methods used to collect and analyse the 2011 bowhead census acoustic array data, and provides a summary of bowhead acoustic activity and locations during selected sub-sample periods. This is one of three critical components of the overall bowhead research program; the other two components are the estimation of visual detection probabilities (Givens *et al.*, 2014) and the estimation of total abundance (Givens *et al.*, 2016), which depends on the combination of acoustic detection and visual detection results. This paper is therefore a cornerstone of the abundance estimate upon which the IWC Scientific Committee bases management advice for this whale stock.

METHODS

Acoustic data collection

Recording arrays

Acoustic data were recorded using arrays of marine autonomous recording units (MARUs) developed by the Cornell Bioacoustics Research Program (Clark *et al.,* 2010). A MARU consists of a digital audio recording system in a positively buoyant glass sphere that can be deployed on the bottom of the ocean for periods of many months. Once deployed, the recorder floats several meters above the sea floor, tethered to an anchor via an acoustically activated release device. A hydrophone mounted outside the sphere transduces sound pressure into an analog electrical signal, which is then filtered, digitised, and stored as a continuous series of time-stamped binary files on an internal hard disk. At the conclusion of a deployment, the recorder's acoustic release device is activated from a recovery vessel, causing the instrument to float to the surface for retrieval.

The MARUs used in this study were programmed to record continuously at a digital audio sampling rate of 2000Hz. The effective acoustic bandwidth of the MARUs, accounting for effects of high-pass and low-pass filters, was 10–800Hz, a frequency range that adequately spans the frequency range of bowhead calls and the lower frequency range of bowhead song notes (Clark and Johnson, 1984; Würsig and Clark, 1993).

[1] *Bioacoustics Research Program, Cornell Lab of Ornithology, Cornell University, Ithaca, NY 14850, USA.*
[2] *Givens Statistical Solutions LLC, 4913 Hinsdale Drive, Fort Collins, CO 80526, USA.*
[3] *North Slope Borough, Department of Wildlife Management, Barrow AK 99723, USA.*

Late on 12 April 2011, a 6m skiff was used to deploy a five-element array of MARUs in a 'zigzag' formation along the edge of the nearshore lead system in the vicinity of the ice-based observation perch. Attempts to deploy buoys more than ≈ 250m north of the perch became impossible because of dangerous ice conditions and –23°C air temperatures. Two additional MARUs were deployed on 1–2 May 2011 by being dropped into the open lead from the nearshore ice edge. One of the five MARUs deployed initially was never retrieved. Because the audio data from differing numbers of MARUs were processed separately, the four MARUs that were recovered from the set deployed on 12 April were considered to comprise a 4-channel array; these four plus the two that were deployed on 2 May comprise a 6-channel array.

Relative positions and details of the individual MARU deployment sites are given in Fig. 1 and Table 1. Depths at the deployment sites varied between 26 and 44m.

Since the two MARUs deployed on 1–2 May were dropped directly from the ice edge, the line connecting their deployment sites was used to define the nominal ice edge for calculating offshore distances of whale locations; the actual ice edge was not perfectly linear. A rectangular zone directly in front of the array is defined as the *aperture zone* (Fig. 1). The aperture zone is the area within which the distribution of offshore distances of acoustic locations is used by Givens *et al.* (2016). One end of the aperture zone is defined by the nominal ice edge. The sides of the aperture zone are perpendicular to the ice edge. The northern side intersects the ice edge at the northernmost MARU position; the southern side intersects the ice edge at a point midway between the two southernmost MARU positions. This midpoint is used, rather than the position of the southernmost MARU, because whale sounds with their first arrival on the southernmost MARU were excluded from the analysis. This is because the vast majority of these sounds are from distant whales approaching the array from the south, and their positions would be in the 30° 'endfire' zone where locations tend to be highly unreliable. Since such locations are discarded later in the analysis process (see below), considerable time was saved in the initial data browsing by skipping such calls. However, if the aperture zone is defined as extending all the way to the southernmost MARU, the exclusion of calls with first arrivals on the southernmost channel would result in the omission of some locations between the two southernmost MARU sites. Using the midpoint between the two southernmost MARUs to define the edge of the aperture zone prevents this omission.

MARUs were retrieved on 27 and 29 July, after the sea ice had retreated from the deployment area. One of the MARU units (Site-5) deployed on 12 April failed to surface in response to the release command and was never recovered.

This is the first time that acoustic monitoring data have been collected beyond the end of the visual census period, which historically has been around 1 June, with end recording dates dictated by ice conditions and whale passage rates.

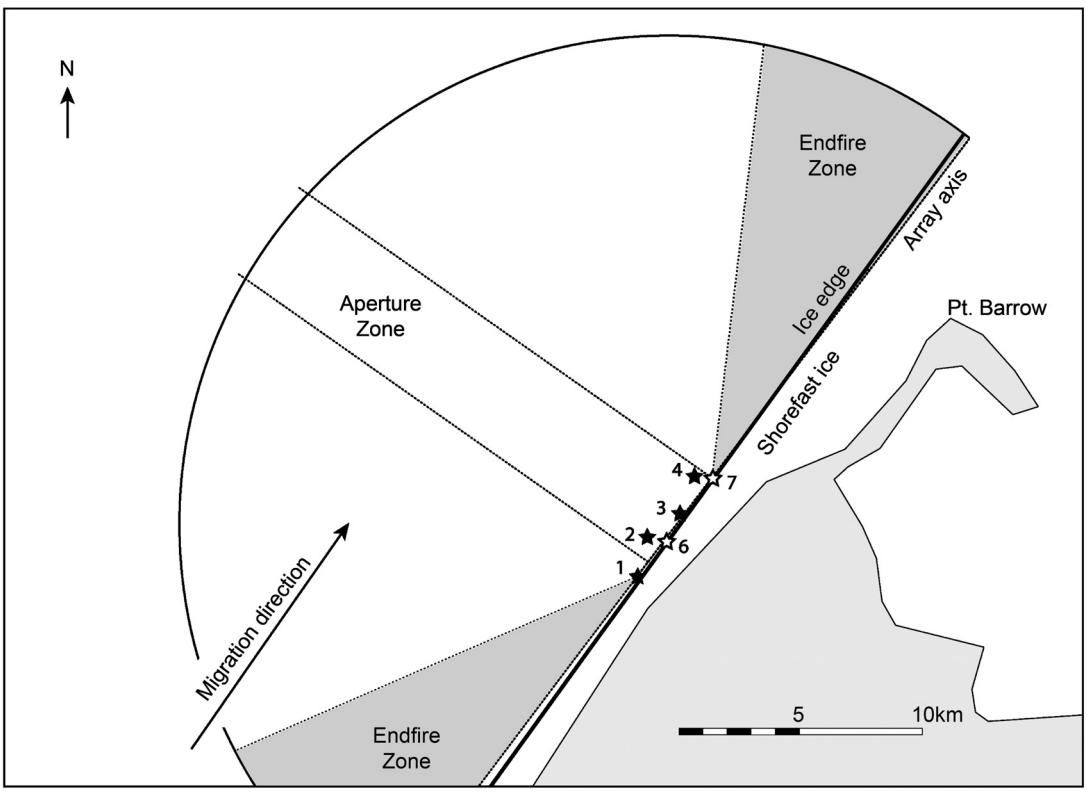

Fig. 1. Passive acoustic arrays deployed near Point Barrow, Alaska. The filled black stars represent MARU positions in the 4-channel array; open stars represent MARUs deployed on 1–2 May to make the 6-channel array. Numbers next to MARU positions are the site numbers as given in Table 1, while noting that Site-5 is not shown because that MARU was not recovered. The large semi-circle (radius = 20km) indicates the area within which acoustic locations were considered reliable. The nominal ice edge used for computing offshore distances is shown. The array axis and aperture zone (see text) are shown for the 6-channel array. For the 4-channel array, the array axis is tilted northward by 8°, and the aperture zone is slightly smaller than shown. The visual observation perch is located 190m from the northernmost MARU (Site-7), too close to be shown separately at this map scale.

Table 1
Locations, depths, deployment and retrieval dates, for MARUs deployed near the visual observation perch in 2011. Approximate depths were obtained from Google Earth.

Site	Latitude (°)	Longitude (°)	Depth (m)	Deployment date	Recovery date
1	71.332717	–156.818367	37	12/04/11	29/07/11
2	71.341383	–156.780300	40	12/04/11	29/07/11
3	71.355267	–156.763767	44	12/04/11	29/07/11
4	71.364067	–156.716650	37	12/04/11	27/07/11
5	71.318367	–156.828800	26	12/04/11	Not recovered
6	71.330967	–156.795800	37	02/05/11	27/07/11
7	71.354533	–156.742783	31	01/05/11	27/07/11

The 4-element MARU array, which provided data for analysis from 0:00[4] on 13 April through 14:59 on 2 May had an array aperture of 4,725m, with distances between adjacent elements of 1,638 to 1,671m. The 6-element array, which recorded from 15:00 on 2 May through 12:00 on 27 July, had an array aperture of 5,065 m, with distances between adjacent elements of 755 to 1,659m. Given the rule of thumb that reliable acoustic locations can be calculated with a linear, sparse array out to ranges four times the array aperture (Carter, 1993), these aperture values support our working assumption that acoustic locations calculated with these arrays are reliable out to approximately 20km from the centre of the arrays.

Array synchronisation

All of the MARUs were synchronised at the start and end of the deployment, and at repeated intervals during the recording period. Synchronisation is required because the algorithm used for computing an acoustic location depends on precise and accurate measurements of the times at which the same sound was recorded by each MARU. Although the quartz-based oscillators that control the audio sampling rates in the MARUs operate at the same nominal frequency, small variations between individual oscillators lead to 'clock drift' among MARUs in the array, which can substantially degrade the accuracy of the relative time-of-arrival measurements.

After recovery of the MARUs a two-step method was used to correct the digital audio files for the effects of MARU-specific clock drift. First, data from onboard temperature loggers were used to compensate for changes in clock frequency that occurred as a result of variations in temperature inside the MARU. Prior to deployment, the oscillator frequency of each MARU was characterised in the laboratory over a wide range of temperatures, yielding a MARU-specific curve of oscillator frequency as a function of temperature. During the deployment period an onboard logger recorded the internal temperature at 15-minute intervals. After the MARUs were recovered, data from each unit's temperature log and its characteristic temperature-frequency curve were used to correct the stream of audio data so that the number of samples in each 15-minute temperature-logging interval matched the value predicted by the nominal sampling rate (Marchetto *et al.,* 2012; see Appendix 3).

The second step in synchronising recordings from MARUs relied on the use of synchronisation sounds played into the water from known locations near the array at intervals of 1 to 8 days (mean = 5) during the deployment period. Because the times of the sync sound playbacks, the speed of sound (1,439m/s), and the distances between the playback speaker and all of the MARUs are known, the expected arrival-times for the sync sound could be calculated for each MARU. After the MARUs were recovered and their data streams were temperature compensated, the observed arrival times of the sync sounds were compared to their expected arrival-times. The number of audio samples between successive recorded sync sounds was adjusted by uniformly inserting or removing samples from the sound stream as necessary to bring the recorded sync sounds to the expected times. Once all of the individual extracted audio data streams were time-compensated in these two ways, they were merged into synchronised, multi-channel audio files for subsequent analysis.

Analysis of acoustic data

Location analysis of the acoustic data was a four-stage process. First, experienced analysts inspected multi-channel spectrograms for selected sample periods and logged bowhead whale sounds that were recorded on three or more MARUs for later location estimation. Sounds recorded on fewer than three MARUs cannot be located and were not logged. Second, an automated localisation algorithm was run as a batch process on the logged whale sounds. Third, the acoustic locations (henceforth 'locations') were screened by a combination of manual and automated processes to eliminate locations that were definitely or probably erroneous. Fourth, locations that were likely to be from the same whale were flagged by an automated algorithm in order to reduce bias from over-represented, acoustically active whales.

The selection of sample periods and the stages in the analysis process are explained in further detail below.

Selection of sample periods

Two sets of sample periods were chosen for location analysis. For the first set, the season was divided into early (13–17 April), gap (18–21 April), core (21 April–15 May), and late (16 May–1 June) time blocks based on major changes in visual sighting rates apparent in the visual field data logs. The gap period corresponds to about three days when no visual watch was possible due to storm conditions. A total of 230 hours of acoustic sample periods was selected within the early, gap, core and late time blocks, with 25, 15, 135 and 55 hours allocated to the early, gap, core and late blocks, respectively. Acoustic sample periods were

[4]All times are given in Alaska Daylight Time.

chosen semi-systematically: taking samples when there was simultaneous visual effort was the highest priority, followed by sampling when the observed whale passage rate was high, and finally ensuring at least some acoustic data had been collected during each time block. Aside from the gap period, all acoustic sampling periods were wholly contained within (potentially longer) periods with visual effort.

The second set of sampling periods was chosen after completing location analysis of the first set of sampling periods and after preliminary analysis of the combined visual and acoustic data from those sample periods. In the analysis of Givens *et al.* (2016), availability (the proportion of whales swimming within 4km of the perch: visual detection range) is estimated from the acoustic data as a smooth function of time. By looking at the preliminary estimated curve, it was possible to identify periods of time when the standard error of the availability estimate was comparatively large. If during this time period, the estimated number of whales passing the perch was also high, then these two factors together could produce an undesirably large contribution of variance to the overall abundance estimate. To reduce this effect, an additional 98 acoustic sampling hours (essentially the maximum the project could fund) were selected in such periods, both within and outside intervals of visual effort. Finally, two additional hours were sampled during visual watch on the first day (13 April) and one additional hour on the last day (1 June) of the analysed season. These were added for purely computational reasons since they enabled estimation of the availability curve over the entire season so that no extrapolation was needed. In sum, 331 hours of acoustic data were sampled. This means that acoustic location analysis was performed for about 28% of the total time acoustically monitored during the analysed visual census period as defined by Givens *et al.* (2016). A complete list of sample periods is provided in Appendix 1.

Manual examination of data and annotation of bowhead sounds

Experienced acoustic analysts used a customised, MATLAB-based software system (XBAT) to examine multi-channel spectrograms of the recorded audio data from each sample period, typically viewing data in the 20–600Hz frequency band, one minute at a time. For the 4-channel array, audio data from MARU sites were assigned channel numbers in the multi-channel sound files from south to north. Thus, channel 1 in the 4-channel spectrograms displayed data from the southernmost MARU, and channel 4 displayed data from the northernmost MARU. For the 6-channel array, audio data from MARU sites were assigned channels in a south to north sequence such that the sequence of sites was 1, 2, 6, 3, 4, 7.

Sounds that were recorded by three or more MARUs were potentially locatable, and were annotated by using a cursor to draw a box around the sound in the one channel that recorded the clearest arrival of the call (i.e. the *reference channel*). Data on the time and frequency boundaries of marked calls were stored in XBAT log files for later processing by the locator algorithm. Calls that were received on fewer than three channels were not logged because they cannot be located.

Three categories of bowhead sounds were marked by analysts (Clark and Johnson, 1984; Würsig and Clark, 1993):

- **Individual calls** (Fig. 2a)**:** Each individual bowhead call that was not part of a call sequence or song (see below) was logged.
- **Call sequences** (Fig. 2b)**:** A call sequence is a sequence of calls, typically frequency-modulated and of similar shape, at regular intervals (typically 1.5–3s) apparently from the same source. Call sequences typically last 20–30s. When call sequences occurred, analysts logged one individual call from each sequence, rather than each individual sound, in order to reduce over-representation of an individual whale in the final data set.

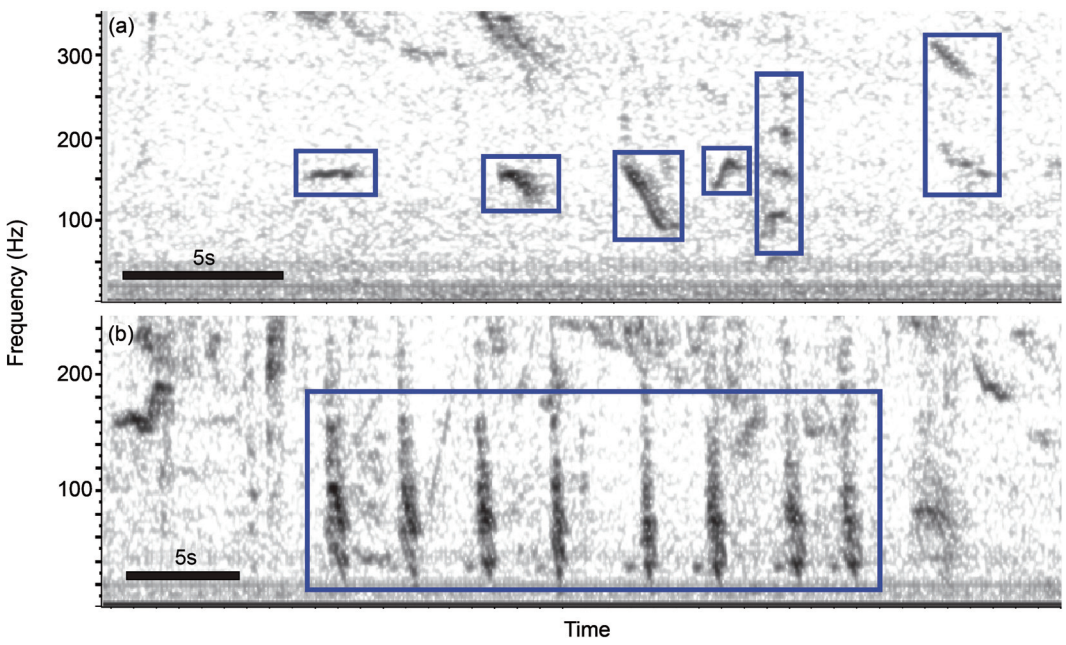

Fig. 2. Examples of individual bowhead whale sounds. Only a single channel of audio recording is shown. (A) Individual calls recorded at 13:49 on 8 May. Note variability of call shapes. (B) A call sequence containing eight calls recorded from a bowhead whale at 23:10 on 29 April. Note the similar shape and regular time intervals of calls within the sequence.

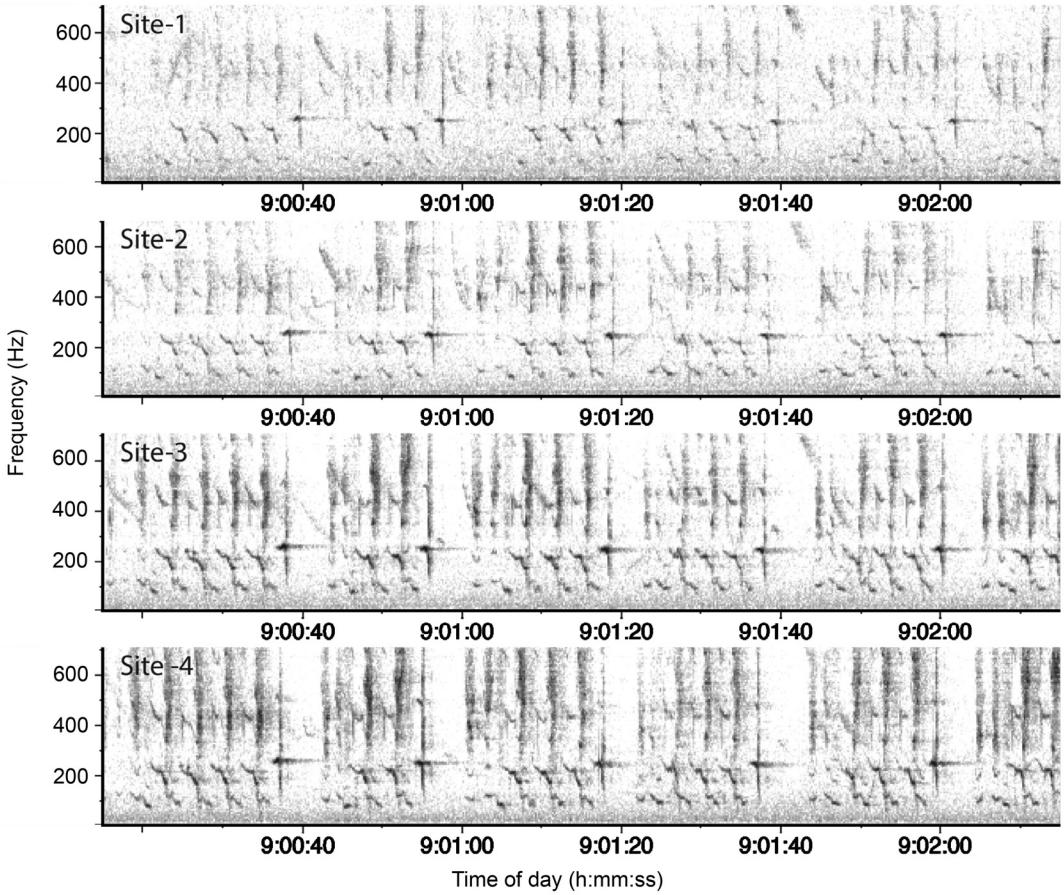

Fig. 3. Example of bowhead whale song recorded at 9:00 on 13 April 2011. Two minutes of the recording are shown from all four MARUs in the recording array. Site-1 is the southernmost recording site in the array (Fig. 1). The highly repetitive structure typical of song is clearly visible.

- **Song (**Fig. 3**):** When bowhead song (Würsig and Clark, 1993; Stafford *et al.,* 2008; Delarue *et al.,* 2009, Tervo *et al.,* 2009) was detected, a single song note was logged once per clock hour. Individual bowhead songs may contain many tens of individual notes within the span of one to two minutes, and individual whales may sing continuously for many tens of minutes or hours at a time. Logging every song note or even a single note from every song could thereby result in orders of magnitude more locations for singing whales than non-singing whales.

In all but the first few sample periods analysed, analysts excluded sounds where the first arrival was on channel 1 (corresponding to the southernmost MARU), because whales producing these sounds would have been to the south of the visual observation perch, and well outside of the rectangular aperture zone used for the abundance estimate (Givens *et al.,* 2016).

Calculation of acoustic locations

When a sound is received on three or more sensors at known positions and in water of known sound velocity, the location of the sound source can be determined from the unique set of pairwise differences in sound's time of arrival at multiple sensors in an array (Clark *et al.,* 1986; Clark *et al.,* 1996; see Fig. 4). In practice, sound source location accuracy and precision are compromised by several sources of uncertainty including sensor position, speed of sound, sound bandwidth and duration, and background noise (see Carter, 1993).

The positions of vocalising bowhead whales were calculated using a custom correlation sum estimation (CSE) algorithm (Urazghildiiev and Clark, 2013), which determines the most likely set of pairwise time-of-arrival differences in order to determine the most likely source location. The CSE locator estimates the most likely set of time delays by finding the pairwise time lags which maximise the sum of filtered waveform cross-correlation values over all sensor pairs. This approach is equivalent to using near-field beamforming spatial energy maximisation to estimate the location of an acoustic source (Appendix 2). The CSE locator software was configured to search for locations out to distances of 20km from the centre of the array. Acoustic locations returned by the locator are expressed in Cartesian coordinates relative to the centroid of the sensor positions. The y-axis of the coordinate system is oriented to geographic (true) North. The locator also returns heuristic estimates of the 95% confidence intervals for x and y coordinates (Appendix 3).

The location algorithms used in previous bowhead censuses determined pairwise arrival-time differences for the same sound recorded on different sensors by finding the maximum in the cross-correlations of, originally, the spectrogram images (Clark *et al.,* 1986), and later, the filtered waveforms (Clark *et al.,* 1996) of the recorded audio. In this approach, time delays are determined independently for each pair of hydrophones, based only on the peak value from the cross-correlation for the corresponding pair of audio channels. The pairwise arrival-time differences were then used as input to an algorithm that calculated the acoustic location (see Clark

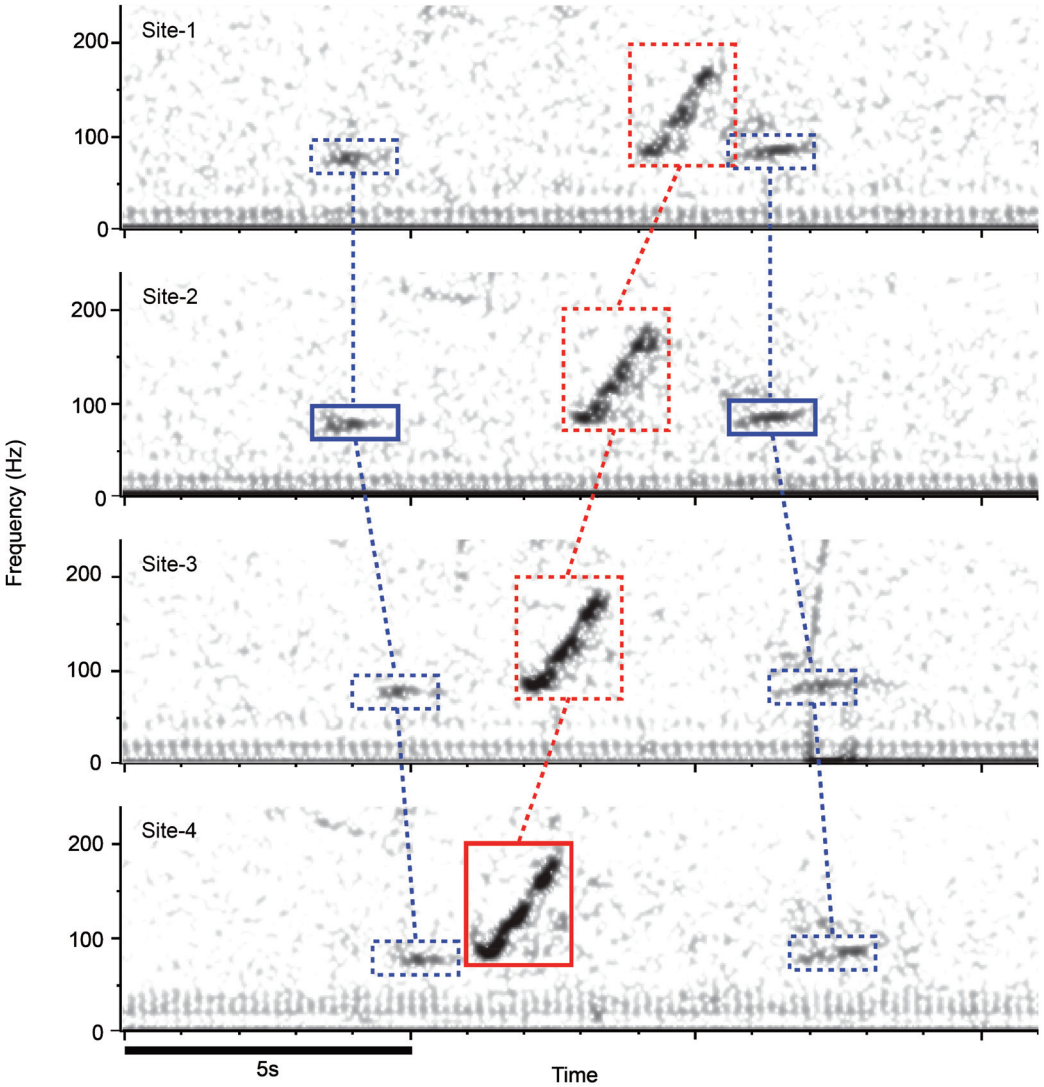

Fig. 4. Time-of-arrival delays for three different bowhead whale calls (boxes) received on the 4-channel recording array at 00:31 on 27 April. The four spectrograms represent synchronised audio streams from four MARU sites, where Site-1 is the southernmost recorder (see Fig. 1). Solid outlines around calls were manually drawn in the 'reference' channel for each call. Dashed outlines around calls in non-reference channels were drawn by the localisation algorithm. Dashed lines link the same call as recorded on the four recorders. The order in which each call was recorded by the four MARUs is determined by the whale's distance from each recorder. The time delays of the first and third calls indicate that they came from approximately the same bearing, nearly equidistant between Site-1 and Site-2. The time delays for the middle call indicate that it came from a different bearing, to the north of the array.

et al., 1996 for a more detailed description). In contrast, the CSE locator determines the most likely time delays by using all of the complete cross-correlation functions for all sensor pairs as an ensemble. This approach is more robust in the presence of noise than traditional peak-picking methods (Birchfield and Gillmor, 2001, 2002).

Review and filtering of automated locations

After all potentially locatable calls in a sample period were manually logged, locations were generated for the logged sounds. One of the outputs of the CSE locator is a prediction of the time at which the logged sound is expected to appear in all channels other than the reference channel, based on the estimated location. XBAT visualises these predicted times of occurrence of secondary arrivals by displaying a coloured rectangular box overlaid on the spectrogram image in each non-reference channel (Fig. 4). If the computed location estimate is correct, these predicted time-delay boxes are properly aligned with the visible arrivals of the whale call in the non-reference channels. Faulty alignment of time delay boxes indicates that the computed location is incorrect, most commonly as a result of poor signal-to-noise ratio on one or more channels. Analysts reviewed each location for faulty time-delays by inspecting the alignment between the predicted time-delay boxes and the images of the whale sound in the non-reference channels. No attempt was made to manually adjust faulty arrival times, and locations that included faulty time-delays were marked in the logs as unreliable and removed from the final data files in a later post-processing step.

After locations with faulty arrival-times were removed, the following additional automated processing was performed via an Excel spreadsheet:

- Locations that fell outside of the 120° sector centered on the line perpendicular to the array axis were excluded from the data set (Clark *et al.,* 1996). In general, with a nearly linear array, location estimates within 30° of the array axis

tend to be unreliable with respect to range, hence are excluded from further analysis. These 30° sectors are called the 'endfire zones' (Fig. 1).

- Range and bearing errors from the centroid of the hydrophone array were calculated for all locations based on the heuristic 95% CIs for *x* and *y*. The *x* and *y* CIs define a rectangular uncertainty area centered on the estimated location. For range error, the difference in range between the estimated location and the farthest corner of this rectangle is used. For bearing error, half the difference between the bearings to the second and third nearest corners of this rectangle is used (Fig. 5). With a linear array, range error generally increases with increasing range; bearing error is largely unaffected by range.
- Locations with bearing errors > 22.5° were flagged as unreliable and excluded from further analysis.
- Offshore distances and minimum and maximum offshore distances were calculated for all locations. The offshore distance for a location is the perpendicular distance from the location to the nominal ice edge (Fig. 1). The minimum and maximum offshore distances are the perpendicular distances from the array axis to the nearest and farthest corners, respectively, of the location's uncertainty rectangle.
- Upon inspection of the complete set of located calls, it became apparent that, in some sample periods, many individual sounds had erroneously been logged for the same song and same call sequences, contrary to the planned protocol. As a result, a few sample periods contained inflated numbers of locations that were probably produced by the same individual whale in a small spatial area and a short period of time. In order to identify these redundant 'duplicate' acoustic location events in the data set without a prohibitively time-consuming manual review of all events, a simple algorithm was developed and applied that identified sequences of events that occurred within 10s of each other and that had overlapping range and bearing errors. Extensive spot-checking of the data marked by this algorithm indicated that most of the events erroneously logged in call sequences and songs were found by this process, with very few cases of properly logged events being identified. Events identified by this algorithm as duplicates were eliminated from further analysis and reporting.

RESULTS

A total of 484 hours of audio data were recorded with the 4-channel array, from 11:00 on 12 April through 15:00 on 2 May. A total of 2,067 hours of audio data were recorded with the 6-channel array from 15:00 on 2 May through 18:00 on 27 July.

A total of 331 hours of data were analysed in 155 sample periods. In total, analysts marked 22,426 sounds that yielded locations in the 120° sector in front of the array. Of these, 3,195 were considered unreliable because their bearing errors were > 22.5°, and 4,393 were identified as likely 10-second duplicates. After removal of the latter two categories of events, a total of 15,647 locations remained. Of these, 6,944 were within the rectangular aperture zone directly in front of the array.

Fig. 6 illustrates the temporal distribution of bowhead acoustic activity over the course of the monitoring season, showing the number of potentially locatable bowhead whale sounds (i.e. sounds that were recorded on ≥3 channels of the acoustic array) per hour for each of the 155 sampling periods. Across all 331 hours analysed, the mean rate of potentially locatable vocalisations was 51.2 sounds/h, including sounds for which locations were deemed unreliable because of excessive bearing error. The figure excludes redundant acoustic location sounds that occurred within 10 s of each other and that had overlapping range and bearing errors; most such 'duplicate' sounds were part of a song or call sequence. The peak rate of vocal activity, 274 sounds/h, occurred between 8:00 and 10:00 on 2 May. The interquartile range of dates in the cumulative distribution of locatable bowhead sounds was between 29 April and 9 May.

Recordings after 1 June have thus far not been systematically sampled to quantify bowhead acoustic activity. However, a few scattered bowhead calls were observed in casual inspection of recordings during the period of 2–10 June, indicating that some bowheads did pass through the census area after the conclusion of the visual census.

Fig. 7 shows the geographic distribution of the 15,647 bowhead sounds located in the 120° sector in front of the array, from the 331 hours of data analysed. Fig. 8 shows the distribution of offshore distances of the 6,944 locations that were within the rectangular aperture zone.

DISCUSSION

Overall, in comparison to recordings from previous censuses, the array recordings made in 2011 had extremely high levels of bowhead whale acoustic activity. Table 2 compares mean rates of occurrence of locatable bowhead sounds in recordings analysed from the 2011 census to data from

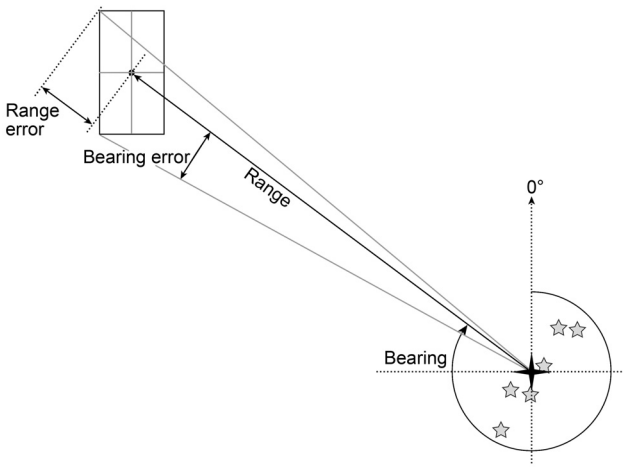

Fig. 5. Schematic illustration of range and bearing to an acoustic location, and their respective errors. The grey stars represent the locations of the MARUs. The black cross represents the centroid of the recording array. The locator algorithm calculates the *x* and *y* coordinates of a vocalising whale (black dot), and the heuristic 95% CIs for *x* and *y*, which define a rectangular uncertainty area. The range and bearing are calculated by converting the *x* and *y* to geographic polar coordinates. The range error is the difference between the range to the location and the farthest corner of the uncertainty rectangle. Bearing error is the difference between the bearing to the location and to either the second or third farthest corners of the uncertainty area.

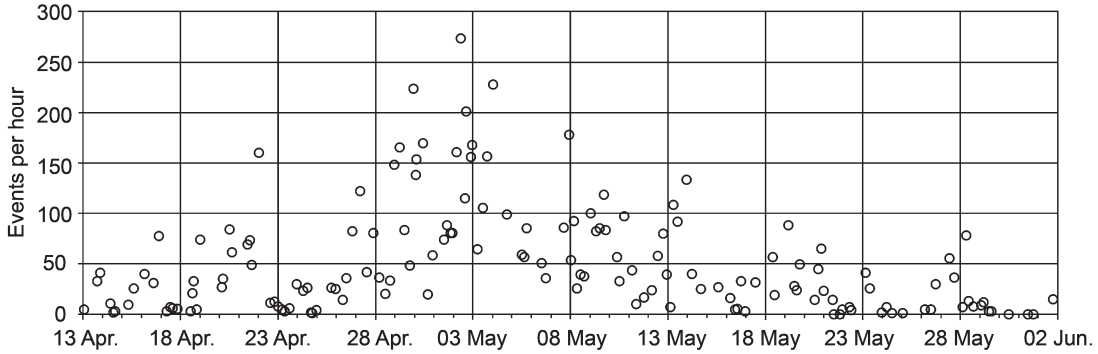

Fig. 6. Mean rate of potentially locatable bowhead whale vocalisations for 155 sample periods between 13 April and 1 June 2011. Each point represents one sample period. Mean length of sample period = 2.16h. Vocalisations that were recorded on < 3 channels of the acoustic array, and could not be located, are not included in these data. In order to convey the seasonal distribution of vocal activity, all vocalisations that were recorded on ≥3 channels of the acoustic array were included in this plot regardless of whether or not they were excluded from location analyses and figures due to excessive bearing error. 'Duplicate' sounds that occurred within 10s of another sound with overlapping range and bearing errors are omitted. The total number of sounds included here = 18,033.

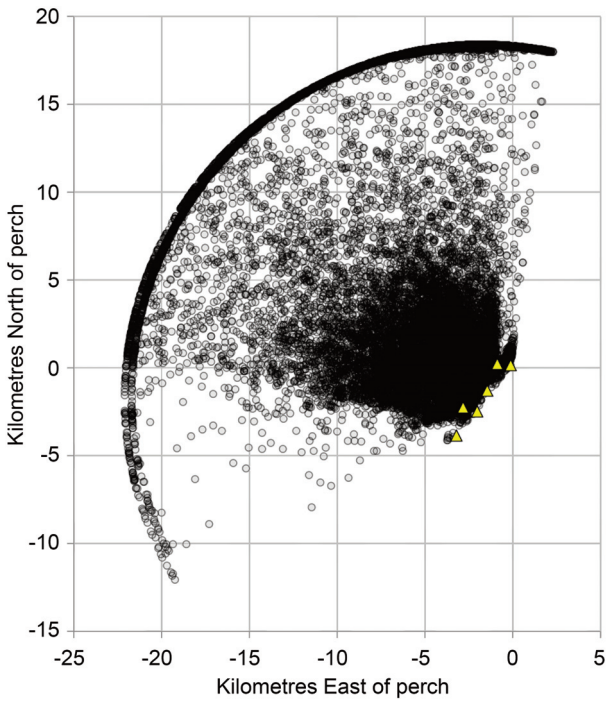

Fig. 7. Acoustic locations of 15,647 bowhead sounds, from 155 sample periods totaling 331 hours of recording between 13 April and 1 June 2011. The origin of the coordinate system is the location of the primary visual perch. Triangles indicate locations of hydrophones in the 6-element recording array. As a whale's true location becomes farther away from the array, range errors inevitably increase. The locator software was configured to search for locations out to 20km, which gives rise to the circular edge in the location distribution. Locations at or close to this 20km boundary represent whales that were probably beyond the 20km search limit.

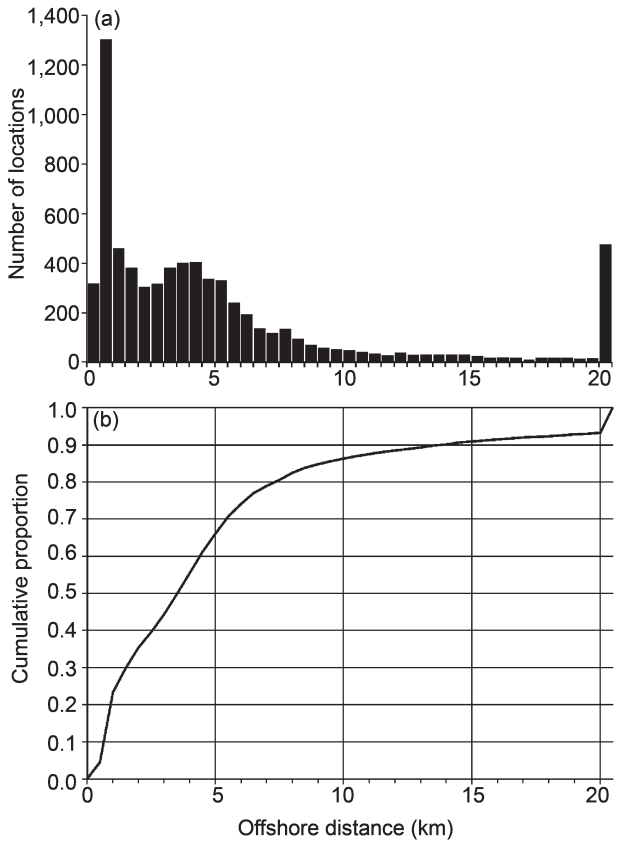

Fig. 8. Offshore distance distribution for the 6,944 locations inside the rectangular aperture zone. (a) Number of locations in 0.5km distance bins. (b) Cumulative proportion of locations ≤ a given distance. In both plots, the greatest value represents all locations at distance > 20km.

1993 and 2001 (Clark and Johnson, 1984; George *et al.,* 2004). Overall, between 1993 and 2011, the mean rate of acoustically located events increased by approximately 570%.

The 2011 recordings also appeared to have much higher occurrence rates of call sequences and songs compared to past censuses, although quantitative comparisons are not presently available.

There were some differences between the methods used in 2011 and in previous years, but it is not believed that these differences account for the increase in acoustic activity or the number of reliable locations. These differences include the use in 2011 of autonomous recorders suspended 2–3m from the seafloor rather than cabled hydrophones deployed over the ice edge or through the ice as in all previous years. For the 2011 data the depths of hydrophones below the surface were 29–42m, while in previous years, hydrophone depths were typically 20–40m. Recorder sensitivity in 2011 was less than that in previous years because MARUs were sampling at 2kHz with a dynamic range of approximately 66dB, while earlier systems were sampling at a minimum of 10kHz with a dynamic range of 90dB. If anything, lower numbers of sound detections would then be expected and fewer acoustic locations from the 2011 system compared to previous years. Array aperture differences were minimal

Table 2

Comparison of numbers of locatable bowhead whale sounds processed from censuses in 1993, 2001 and 2011.

	1993	2001	2011
Hours analysed	732	757	331
Reliable locations	6,042	26,606	15,647
Locations/h	8.3	35.1	47.3

between 2011 and previous years, where array aperture influences the range out to which locations are reliable. In 2011 array apertures were 4,725m (4-channel) and 5,065m (6-channel); in 1993 apertures of the 25 separate arrays used were typically around 4,425m. Thus, the 4- and 6-channel arrays used in 2011 were around 7% and 14% longer than those used in 1993.

This paper is the final cornerstone of the 2011 BCB bowhead ice-based abundance estimate (Givens *et al.*, 2016). Although that estimate is quite complex, its essence is that it scales up counts of sighted whales by adjusting for detection probability (sighting a whale given that it is available to be sighted; see Givens *et al.,* 2014) and availability (whether a whale passing the perches is available to be sighted, i.e. within 4km of the ice edge). The acoustic analyses presented here provide the sole basis for the availability correction and hence are essential for estimating abundance. In particular, the availability correction is estimated as a time-varying smooth function of the probability that animals pass within visual range of the observation stations, where those probabilities are derived from the data presented here. Uncertainty is estimated using the bootstrap.

Abundance estimates for the BCB bowhead population are required for IWC management of subsistence hunting by Alaska Natives. Sustainable quotas are estimated using the IWC's Bowhead *Strike Limit Algorithm* (*SLA*; IWC, 2003) which requires updated abundance estimates every 10 years or, ideally, much more frequently. The prior two abundance estimates were for 2001 (Zeh and Punt, 2005) and 2004 (Koski *et al.,* 2010); the next is planned for 2019.

Our acoustic results suggest that BCB bowhead abundance has markedly increased in the last two decades, and it is not believed that any of the differences in field data collection and/or data processing methods can account for the almost 6-fold increase in rates of locatable bowhead sounds observed in 2011 in comparison to 1993. Moreover, the past four fully corrected abundance point estimates have been 7,778 (1993), 10,470 (2001), 12,631 (2004) and 16,820 (2011). This also suggests that the bowhead population is growing relatively rapidly despite the small subsistence harvest and profound changes in the arctic habitat.

ACKNOWLEDGEMENTS

The many researchers who worked on the ice-based visual and acoustic survey collecting the data required for the abundance estimate are gratefully acknowleged. In particular, people recognised are Jason Michalec, Jason Herreman, Kate Stafford, and Billy Adams who helped deploy and retrieve the acoustic recorders under very dangerous conditions. The Whaling Captains Association at Barrow and the Alaska Eskimo Whaling Commission are thanked for their support and patience, allowing us to conduct these studies near Utqiagvik (formerly Barrow) during the whaling season. Kristin Hodge, Maureen Loman, Clara MacCarald, Elizabeth McDonald, and Kaitlin Palmer are thanked for painstaking analysis of the acoustic data. We thank Mike Pitzrick for software tools and consultation on post-processing of the location data. We also thank the North Slope Borough, NOAA, BOEM, and BP Exploration, Alaska, Inc. for funding by which to collect and analyse the acoustic data used for the abundance estimate.

REFERENCES

Birchfield, S.T. and Gillmor, D.K. 2001. Acoustic source direction by hemisphere sampling. Presented to the IEEE International Conference on Acoustics, Speech, and Signal Processing (ICASSP*)*, 7–11 May 2001, Salt Lake City, UT, USA. 4pp.

Birchfield, S.T. and Gillmor, D.K. 2002. Fast Bayesian acoustic localization. Presented to the IEEE International Conference on Acoustics, Speech, and Signal Processing (ICASSP), 13–17 May 2002, Orlando, FL, USA. 4pp.

Carter, G.C. (Ed.) 1993. *Coherence and Time Delay Estimation: An Applied Tutorial for Research, Development, Test, and Evaluation Engineers*. IEEE Press. 518pp.

Clark, C.W., Brown, M.W. and Corkeron, P. 2010. Visual and acoustic surveys for North Atlantic right whales, *Eubalaena glacialis*, in Cape Cod Bay, Massachusetts, 2001–2005: Management implications. *Mar. Mamm. Sci.* 26: 837–54.

Clark, C.W., Charif, R.A., Mitchell, S. and Colby, J. 1996. Distribution and behavior of the bowhead whale, *Balaena mysticetus*, based on analysis of acoustic data collected during the 1993 spring migration off Point Barrow, Alaska. *Rep. int. Whal. Commn* 46: 541–52.

Clark, C.W., Ellison, W.T. and Beeman, K. 1986. Acoustic tracking of migrating bowhead whales. *Oceans 86*: 341–6. [Available from IEEE Oceanic Engineering Society]:

Clark, C.W. and. Johnson, J.H. 1984. The sounds of the bowhead whale, *Balaena mysticetus*, during the spring migrations of 1979 and 1980. *Can. J. Zool.* 62: 1,436–41.

Delarue, J., Laurinolli, M. and Martin, B.. 2009. Bowhead whale (*Balaena mysticetus*) songs in the Chukchi Sea between October 2007 and May 2008. *J. Acoust. Soc. Am.* 126: 3,319–28.

George, J.C., Zeh, J., Suydam, R.S. and Clark, C.W. 2004. Abundance and population trend (1978–2001) of western Arctic bowhead whales surveyed near Barrow, Alaska. *Mar. Mam. Sci.* 20: 755–73.

Givens, G.H., Edmondson, S.L., George, J.C., Suydam, R., Charif, R.A., Rahaman, A., Hawthorne, D.L., Tudor, B., Delong, R.A. and Clark, C.W. 2016. Horvitz-Thompson whale abundance estimation adjusting for uncertain recapture, temporal availability variation and intermittent effort. *Environmetrics*, 26: 1–16.

Givens, G.H., Edmondson, S.L., George, J.C., Tudor, B., DeLong, R.A. and Suydam, R. 2014. Weighted likelihood recapture estimation of detection probabilities from an ice-based survey of bowhead whales. *Environmetrics*, 26: 1–16.

International Whaling Commission. 2003. Report of the Scientific Committee. *J. Cetacean Res. Manage. (Suppl.)* 5:1–92.

Koski, W.R., Zeh, J. Mocklin, J., Davis A.R., Rugh, D.J., George, J.C. and Suydam, R. 2010. Abundance of Bering-Chukchi-Beaufort bowhead whales (*Balaena mysticetus*) in 2004 estimated from photo-identification data. *J. Cetacean Res. Manage.* 11(2): 89–99.

Marchetto, P., Strickhart, A., Mack, R. and Cheyne, H. 2012. Temperature compensation of a quartz tuning-fork clock crystal via post-processing. Presented to the IEEE International Frequency Control Symposium (FCS), 20–24 May 2012. Baltimore, MD, USA. 4pp.

Stafford, K.M., Moore, S.E., Laidre, K.L and Heide-Jorgensen, M.P. 2008. Bowhead whale springtime song off West Greenland. *J. Acoust. Soc. Am.* 124: 3,315–23.

Tervo, O.M., Parks, S.E. and Miller, L.A. 2009. Seasonal changes in the vocal behavior of bowhead whales (*Balaena mysticetus*) in Disko Bay, Western Greenland. *J. Acoust. Soc. Am.* 126: 1,570–80.

Urazghildiiev, I.R. and Clark, C.W. 2013. Comparative analysis of localization algorithms with application to passive acoustic monitoring. *J. Acoust. Soc. Am.* 134: 4,418–26.

Würsig, B. and Clark, C.W. 1993. Behavior. pp.157–199. *In*: J. J. Burns, J. J. Montague and C. J. Cowles (ed.) *The Bowhead Whale*. Chapter 5, Special Publication No. 2. The Society for Marine Mammalogy.

Zeh, J. and Punt, A. 2005. Updated 1978–2001 abundance estimates and their correlations for the Bering-Chukchi-Beaufort Seas stock of bowhead whales. *J. Cetacean Res. Manage.* 7(2): 169–75.

Appendix 1. Sample periods for acoustic analysis

Date	Start time	End time	Duration (h)	Date	Start time	End time	Duration (h)
13/04	0:00	2:00	2.0	27/04	4:00	7:00	3.0
13/04	15:44	18:30	2.8	27/04	10:18	16:18	6.0
13/04	20:00	22:00	2.0	27/04	20:00	22:00	2.0
14/04	8:32	10:32	2.0	28/04	4:00	6:00	2.0
14/04	12:38	13:38	1.0	28/04	10:00	14:00	4.0
14/04	14:34	16:34	2.0	28/04	16:00	20:00	4.0
15/04	6:38	8:38	2.0	28/04	22:00	23:59	2.0
15/04	13:12	15:12	2.0	29/04	4:00	7:00	3.0
16/04	3:00	4:00	1.0	29/04	10:00	14:00	4.0
16/04	13:30	15:30	2.0	29/04	16:00	20:00	4.0
16/04	20:30	22:30	2.0	29/04	22:00	23:59	2.0
17/04	6:15	8:15	2.0	30/04	1:00	2:00	1.0
17/04	11:00	12:00	1.0	30/04	2:00	3:30	1.5
17/04	13:00	16:17	3.3	30/04	8:30	12:30	4.0
17/04	20:03	21:00	0.9	30/04	14:30	18:30	4.0
18/04	12:00	13:00	1.0	30/04	21:00	23:00	2.0
18/04	14:00	15:00	1.0	1/05	12:00	13:00	1.0
18/04	16:00	17:00	1.0	1/05	14:08	18:12	4.1
18/04	18:00	21:00	3.0	1/05	20:00	21:00	1.0
19/04	0:00	1:00	1.0	1/05	22:00	23:59	2.0
20/04	2:00	3:00	1.0	2/05	2:00	5:00	3.0
20/04	4:00	5:00	1.0	2/05	8:00	10:00	2.0
20/04	12:00	13:00	1.0	2/05	13:00	14:59	2.0
20/04	14:00	17:00	3.0	2/05	15:00	16:00	1.0
21/04	10:00	11:00	1.0	2/05	21:00	22:00	1.0
21/04	13:00	14:00	1.0	2/05	22:00	23:59	2.0
21/04	14:55	16:05	1.2	3/05	4:00	7:00	3.0
22/04	0:00	1:00	1.0	3/05	10:00	14:00	4.0
22/04	10:30	18:00	7.5	3/05	15:00	19:50	4.8
22/04	19:00	21:00	2.0	4/05	0:00	1:00	1.0
23/04	0:00	0:15	0.3	4/05	17:00	18:00	1.0
23/04	5:00	6:00	1.0	5/05	10:10	14:00	3.8
23/04	8:00	9:00	1.0	5/05	14:40	15:15	0.6
23/04	10:10	18:00	7.8	5/05	16:17	20:00	3.7
23/04	22:00	23:59	2.0	6/05	10:10	14:11	4.0
24/04	6:00	8:00	2.0	6/05	16:01	20:00	4.0
24/04	10:00	14:00	4.0	7/05	14:00	17:00	3.0
24/04	15:00	18:00	3.0	7/05	21:00	23:59	3.0
24/04	18:00	19:00	1.0	8/05	0:00	2:00	2.0
24/04	22:00	23:59	2.0	8/05	3:00	5:00	2.0
25/04	16:00	19:00	3.0	8/05	7:00	9:00	2.0
25/04	22:00	23:59	2.0	8/05	10:49	14:03	3.2
26/04	7:00	9:00	2.0	8/05	16:00	18:17	2.3
26/04	10:17	14:00	3.7	9/05	0:00	2:00	2.0
26/04	18:00	21:00	3.0	9/05	7:00	9:00	2.0
9/05	10:03	14:00	4.0	20/05	16:00	18:00	2.0
9/05	15:57	17:51	1.9	20/05	20:00	22:00	2.0
9/05	18:30	21:00	2.5	20/05	23:00	23:59	1.0
10/05	9:00	10:20	1.3	21/05	10:00	11:00	1.0
10/05	10:20	14:00	3.7	21/05	12:00	13:00	1.0
10/05	16:00	20:00	4.0	21/05	19:00	21:00	2.0
11/05	3:00	5:00	2.0	21/05	21:30	23:30	2.0
11/05	8:30	10:00	1.5	22/05	7:00	8:00	1.0
11/05	16:00	21:00	5.0	22/05	9:00	10:00	1.0
12/05	3:00	5:00	2.0	23/05	3:00	4:00	1.0
12/05	9:00	14:00	5.0	23/05	8:00	8:59	1.0
12/05	16:00	20:00	4.0	23/05	23:00	23:59	1.0
12/05	22:00	23:59	2.0	24/05	5:00	6:00	1.0
13/05	2:00	4:00	2.0	24/05	10:00	14:00	4.0
13/05	6:00	8:00	2.0	25/05	0:00	2:00	2.0
13/05	10:02	14:00	4.0	26/05	4:00	5:00	1.0
13/05	22:00	23:59	2.0	26/05	11:00	12:00	1.0
14/05	5:00	6:00	1.0	26/05	17:00	18:00	1.0
14/05	16:00	18:00	2.0	27/05	10:00	12:00	2.0
15/05	14:00	14:40	0.7	27/05	16:00	17:00	1.0
16/05	4:00	5:00	1.0	28/05	2:00	3:00	1.0
16/05	10:02	10:50	0.8	28/05	7:00	8:00	1.0
16/05	12:45	14:00	1.3	28/05	10:00	11:00	1.0
16/05	16:00	20:00	4.0	28/05	15:00	17:00	2.0
16/05	23:00	23:59	1.0	29/05	1:00	2:00	1.0
17/05	10:02	14:00	4.0	29/05	4:00	5:00	1.0
18/05	8:00	10:00	2.0	29/05	11:00	12:00	1.0
18/05	11:00	12:00	1.0	29/05	14:00	15:00	1.0
19/05	4:00	5:00	1.0	30/05	11:00	12:00	1.0
19/05	10:00	13:00	3.0	31/05	10:00	12:00	2.0
19/05	14:00	15:00	1.0	31/05	17:00	18:00	1.0
19/05	17:00	19:00	2.0	1/06	17:00	18:00	1.0
20/05	12:00	13:00	1.0	1/06	18:00	19:00	1.0

Appendix 2. The Correlation Sum Estimation (CSE) algorithm

The correlation sum estimation (CSE) locator employs near-field beamforming spatial energy maximisation to estimate the location of an acoustic source. The formulation here is mathematically similar to that employed by Birchfield and Gillmore (2001, 2002) to study the localisation of acoustic sources in a room, although here bearing and range are computed, rather than azimuth and elevation as computed by those authors. Given N sensors, the average power output of an M sample record of a conventional delay and sum beamformer with a narrow band signal at frequency ω emitted from spatial location $\vec{x}$ is given by

$$P(\vec{x}) = \frac{1}{M}\sum_{k=1}^{M}\sum_{n=1}^{N}\sum_{m=1}^{N} y_n(k)y_m^*(k)e^{i\omega(\tau_n(\vec{x})-\tau_m(\vec{x}))}$$

where $\tau_n(\vec{x})$ is the propagation time from location $\vec{x}$ to sensor n, and $y_n(k)$ is the signal received at sensor n at discrete sample time k. Observing that in the phasor domain, the complex exponential represents a time shift operator, and exchanging the order of the summations, it may be written

$$P(\vec{x}) = \frac{1}{M}\sum_{n=1}^{N}\sum_{m=1}^{N}\left[\sum_{k=1}^{M} y_n(k)y_m^*\left(k-\frac{\tau_n(\vec{x})-\tau_m(\vec{x})}{T}\right)\right]$$

The quantity in brackets is observed as the M point cross-correlation of $y_n(k)$ and $y_m(k)$ evaluated at discrete sample time $\frac{\tau_n(\vec{x})-\tau_m(\vec{x})}{T}$. That is,

$$P(\vec{x}) = \frac{1}{M}\sum_{n=1}^{N}\sum_{m=1}^{N} Corr(y_n y_m)\,|_{\frac{(\tau_n(\vec{x})-\tau_m(\vec{x})}{T}}$$

where T is the temporal sample period. It is physically intuitive that the value of $\vec{x}$, which maximises this sum, corresponds to the location of the source. One advantage to this technique is that the entire set of pair-wise cross-correlation functions may be pre-computed in the frequency domain using the Fast Fourier Transform (FFT), which is much more computationally efficient than computation in the time domain. When searching space for the point of maximum power, the correlation values in a series of tables are merely looked up, requiring no further correlation computation. If the maximum value of a pair-wise cross-correlation function does not exceed a prescribed threshold value, then that pair is excluded from the sum. If the number of remaining channels does not exceed a prescribed number, then failure is indicated and the calculation is aborted.

The remainder of the algorithm consists of a stochastic search over space to find the point of maximum average power. Initially, 30,000 points are randomly chosen inside a circle of radius R centred at the origin. The average power is calculated at each point and the point $\hat{\vec{x}}$ of maximum power is located. The centroid of the set $\sum\vec{x}_i$ is also computed. The procedure is iterated with the circle centered at the point of maximum power observed over all previous iterations and a radius equal to the centroid magnitude of the previous iteration. The procedure continues until the magnitude of the centroid is less than a prescribed value.

Appendix 3. Error estimation in the Correlation Sum Estimation (CSE) locator v2.3

Estimation of standard errors and confidence intervals for the location estimates produced by the CSE locator is extremely complex. Below, a heuristic approach is decribed. An advantage of this approach is that it allows us to incorporate more sources of uncertainty, including statistical 'process errors' beyond standard sampling/estimation error. A disadvantage is that there is no assurance that the resulting confidence interval actually has 95% coverage. Due to this concern, the intervals are referred to as 'heuristic 95% confidence intervals' to distinguish them from 95% confidence intervals derived directly from statistical theory.

Although the true coverage probability of these CIs may be only approximately correct, a relatively large degree of coverage rate error can be tolerated for the present purpose. Specifically, for the population abundance estimate of Givens *et al.* (2013), the CIs produced here are used only to estimate weights for time-smoothing probabilities that offshore distances exceed 4km. The estimated smooth probability is fairly insensitive to the choice of weights. Furthermore, in any time interval (say, 1h), let us suppose that the CI coverage probabilities are relatively inaccurate but such inaccuracies are not correlated with offshore distance. Admittedly this may be a strong assumption, but to the extent that it is true, the errors in the weights employed at the local smooth fit for this time interval would tend to cancel each other out, thereby leaving the smooth fit relatively unbiased.

Now for the discussion of the components of uncertainty reflected in our heuristic estimates of standard errors and confidence intervals for locations.

(1) Sources of location error

The major sources of error in the CSE locator algorithm are:

(a) Statistical error

The CSE locator operates by maximisation of the sum of pair-wise correlations of the array's sensors. The acoustic data from each sensor include noise. The statistical error measures how much the noise affects the location estimate.

(b) Error due to sensor positional uncertainty

The CSE locator algorithm assumes that the locations of the sensors are known exactly; in reality, this is never true.

(c) Error due to variation in the speed of sound

Like the sensor positions, the CSE locator algorithm assumes that the speed of sound is known with great accuracy. In marine environments this could become a significant source of error.

(d) Error due to uncertainty in the sensors' clock rates

Clock rate uncertainty can be mitigated to some degree by aligning the sensor recordings with respect to a bang or an FM sweep, and amortising the error uniformly across the sensor recordings between the

start and end markers. De-convolving the sensor unit's oscillator crystal temperature history can also mitigate temperature-induce clock rate drift.

2. Error estimation

(a) Statistical location error

The question here is 'Given the (noisy) sensor data, how accurately is the location of the energy maximum known?' Accordingly, our goal is to compute the variance of the energy maximum location estimator $\hat{\vec{x}}$. While searching for an energy maximum, the CSE locator maintains a list of the top 1,000 highest candidate energies and coordinates. The location estimator variance was estimated by computing the sample variance of this set.

$$\sigma_x^2 = \frac{1}{N-1}\sum (x_i - \bar{x})^2$$

The same approach is used for σ_y^2 and (optionally) σ_z^2.

Confidence intervals for x, y, and z are constructed independently using Gaussian assumptions. (The possible alternative approach based on a histogram of the 1,000 candidates is a topic for future work.) This study has not yet implemented a non-independent approach based on a multivariate Gaussian approach for the three coordinates jointly.

(b) Systematic location error due to sensor position uncertainties

Systematic error due to sensor position uncertainty is estimated using numerical sensitivities of the error maximum with respect to small changes in the sensor positions. To obtain the coordinate confidence limits, this study employs a first order Taylor expansion of the energy as a function of location vector $\vec{x}$:

$$E = E(\vec{x}^{\max}) + \delta\vec{x}\cdot\nabla_{\vec{x}'}E(\vec{x}')|_{\vec{x}'=\vec{x}^{\max}} + \text{higher order terms}$$

Taking, for example, the x component, to first order it is

$$E = E(\vec{x}^{\max}) + \delta x\frac{\partial}{\partial x'}E(\vec{x}')|_{\vec{x}'=\vec{x}^{\max}}$$

Unfortunately, for a true maximum of the energy function, the derivative $\frac{\partial}{\partial x'}E(\vec{x}')|_{\vec{x}'=\vec{x}^{\max}}$ is zero. However, the first order representation is linear in δx, approximating the energy surface as a cone with a constant slope along each coordinate axis. Therefore, if a suitable point away from the energy maximum at the apex of the cone was chosen, the partial derivative can be numerically estimated $\frac{\partial}{\partial x'}E(x)$. Conveniently, the CSE locator supplies us with an appropriate distance scale, the median centroid distance, d. The choice was made to compute the numerical derivative at distances $\Delta x = \Delta y = \Delta z = \frac{d}{2}$ from the energy maximum.

Numerical calculations of the derivatives can be very difficult to compute; the simple two point $\frac{\Delta y}{\Delta x}$ is frequently not accurate enough and it gives no bounds on the accuracy. Ridder's method was chosen to compute the derivatives and a bound on their errors. Conceptually, Ridder's method computes the ratio $\frac{\Delta y}{\Delta x}$ for a decreasing series of Δx and extrapolates to $\Delta x = 0$. If the error bound returned by Ridder's method is larger than the derivative estimate, the CSE locator displays a warning message, but does not signal failure.

It was sought to compute the sensitivity of the source location with respect to the change in sensor position location $\vec{s}_i$. Concentrating on the x component of the ith sensor position vector and invoking the chain rule for partial derivatives

$$\frac{\partial x}{\partial s_{i,x}} = \frac{\partial E}{\partial s_{i,x}}\frac{\partial x}{\partial E}$$

$$\frac{\partial x}{\partial s_{i,x}} = \frac{\frac{\partial E}{\partial s_{i,x}}}{\frac{\partial E}{\partial x}}$$

This is the sensitivity of location coordinate, x, with respect to the ith sensor position coordinate $s_{i,x}$. The partial derivatives appearing in the numerator and denominator are estimated using Ridder's method. For a finite uncertainty in the ith sensor position's coordinate, $\Delta s_{i,x}$, the change is computed in x, Δx, to be

$$\Delta x = \frac{\frac{\partial E}{\partial s_{i,x}}}{\frac{\partial E}{\partial x}}\Delta s_{i,x}$$

which is the error estimate that is sought. Assuming the input of 95% confidence limit of $\Delta s_{i,x}$, The 95% confidence limit of Δx was obtained. The CSE locator repeats this calculation for the x, y and (optionally) z position components for each sensor used in the calculation of the energy (i.e. the correlation sum). A similar calculation is performed to obtain an estimate of the uncertainty in the location coordinates due to uncertainty in the speed of sound. Finally, the errors are summed coherently by components to obtain an estimate of the upper bound of the uncertainty in the energy maximum location.

(c) Systematic location error due to speed of sound uncertainty

The systematic error due to the uncertainty in the speed of sound is estimated using the same methodology used to estimate the systematic error due to uncertainties in the sensor locations.

(d) Clock drift error

Due to temperature changes and aging of the crystal oscillators, MARU clocks may drift over time by rates of several seconds per day. MARU data extraction software mitigates the error in two ways: (1) oscillator temperatures are logged during the duration of the deployment and acoustic data are compensated for temperature drift using a function measured in the laboratory, and (2) any residual error is amortised over the interval between synchronisation points. Amortisation of a few seconds per day is actually a very small correction. For example, assume the clock drift was –3 sec/day. Since there are 86400 sec/day, one audio frame must be inserted every $\frac{86400}{3}$ = 28800 frames, a minor correction. By amortising the error this way, it is never more than one sample period away from the correct absolute time. Therefore, it is believed that it is justified to ignore clock drift error.